SPARC 4th General Assembly 31 August – 5 September 2008
Bologna, Italy

General Aspects of a T213L256 middle atmosphere general circulation model

Shingo Watanabe[1], Yoshio Kawatani[1], Yoshihiro Tomikawa[2], Kazuyuki Miyazaki[1], Masaaki Takahashi[3&1], and Kaoru Sato[4]
(KANTO project members)

1 : Frontier Research Center for Global Change/ Japan Agency for Marine-Earth Science and Technology
2: National Institute of Polar Research
3: Center for Climate System Research, Univ. of Tokyo
4: Department of Earth and Planetary Science, Graduate school of Science, Univ. of Tokyo
E-mail: wnabe@jamstec.go.jp

This study was supported by Innovative Program of Climate Change, MEXT, Japan.

*J. Geophys. Res. ,113, D12110, doi:10.1029/2008JD010026.

Abstract

- A high-resolution middle atmosphere general circulation model (GCM) developed for studying small-scale atmospheric processes is presented, and the general features of the model are discussed. The GCM has T213 horizontal resolution and 256 vertical levels extending from the surface to a height of 85 km with a uniform vertical spacing of 300 m. Gravity waves (GWs) are spontaneously generated by convection, topography, instability, and adjustment processes in the model, and the GCM reproduces realistic general circulation in the extratropical stratosphere and mesosphere. The oscillations similar to the stratopause semi-annual oscillation and the quasi-biennial oscillation (QBO) in the equatorial lower stratosphere are also spontaneously generated in the GCM, although the period of the QBO-like oscillation is short (15 months). The relative roles of planetary waves, large-scale GWs, and small-scale GWs in maintenance of the meridional structures of the zonal wind jets in the middle atmosphere are evaluated by calculating Eliassen-Palm diagnostics separately for each of these three groups of waves. Small-scale GWs are found to cause deceleration of the wintertime polar night jet and the summertime easterly jet in the mesosphere, while extratropical planetary waves primarily cause deceleration of the polar night jet below a height of approximately 60 km. The meridional distribution and propagation of small-scale GWs are shown to affect the shape of the upper part of mesospheric jets. The phase structures of orographic GWs over the South Andes and GWs emitted from the tropospheric jet stream are discussed as examples of realistic GWs reproduced by the T213L256 GCM.

Background

- Middle atmosphere studies using GW resolving GCMs
  - GFDL SKYHI GCM (N270 0.33 deg)

    Hamilton et al. (1999), Koshyk et al. (1999)
    - Realistic PNJ in SH winter
    - Realistic horizontal wavenumber spectra of GW energy
  - CCSR/NIES AGCM (T106L53 Aqua Planet)

    Sato et al. (1999)
    - Dominance of GWs with frequencies near inertial frequency at each latitude
    - Meridional (V-shaped) propagation of GWs from tropical convection
    - Downward propagating GWs from PNJ

- New observations and GW parameterizations
  - Satellite observations of GWs

    MLS, MSX, CRISTA, AMSU-A, HRIDLS, AIRS, SABER, GPS..
  - Spectral GW parameterizations

    Hines(1997), Warner and McIntyre (1996), Alexander and Dunkerton(1999)
  - Parameterizations specifying non-orographic GW source spectra

    Chung and Baig (1998), Beres et al.(2004), Sharron and Manzini (2002)
  - Ray-based GW parameterization considering lateral propagation across model grids

- T213 GCM with high vertical resolution
  - Extremely high horizontal resolution GCM (Δh = 10-20 km) is still too expensive to conduct multi-year simulations.
  - During vertical propagation of atmospheric waves, their wave parameters (e.g., λz) continuously change with vertical shear of the background winds and static stability variation.
  - Vertical change in Δz causes artificial deformation of atmospheric waves.
  - High vertical resolution is useful to compare model results with observations, and to interpret observed phenomena.

Model

- AGCM of a coupled climate model MIROC3.2 collaboratively developed at CCSR / NIES / FRCGC.
- Horizontal resolution:

  T213 ($\Delta\lambda$~0.56°, λ_{min}~188 km)
- Vertical resolution:

  300 m (256 Levels between 0~85 km)
- Hybrid σ-p vertical coordinate system
- Radiation: mstrnX (*Sekiguchi and Nakajima* 2007) Based on the two-stream discrete ordinate method and a correlated k-distribution method. (High resolution band separation method with very high accuracy)
- Cumulus: prognostic Arakawa-Schubert scheme with an empirical cumulus suppression condition, which allows organization of grid-scale convection
- Large-scale condensation: prognostic liquid cloud water (diagnostic partition of liquid/ice clouds)
- **GWD parameterizations : off Resolved waves only!**
- Richardson number dependent vertical diffusion (Mellor-Yamada level 2.0)
- Three soil layer, simple bucket model for hydrology
- Bottom boundary conditions: Realistic topography, AMIP-I SST and sea ice
- Integration period: 3 years
- January in the 2nd year and July in the 1st year are analyzed in this study.

Mean fields

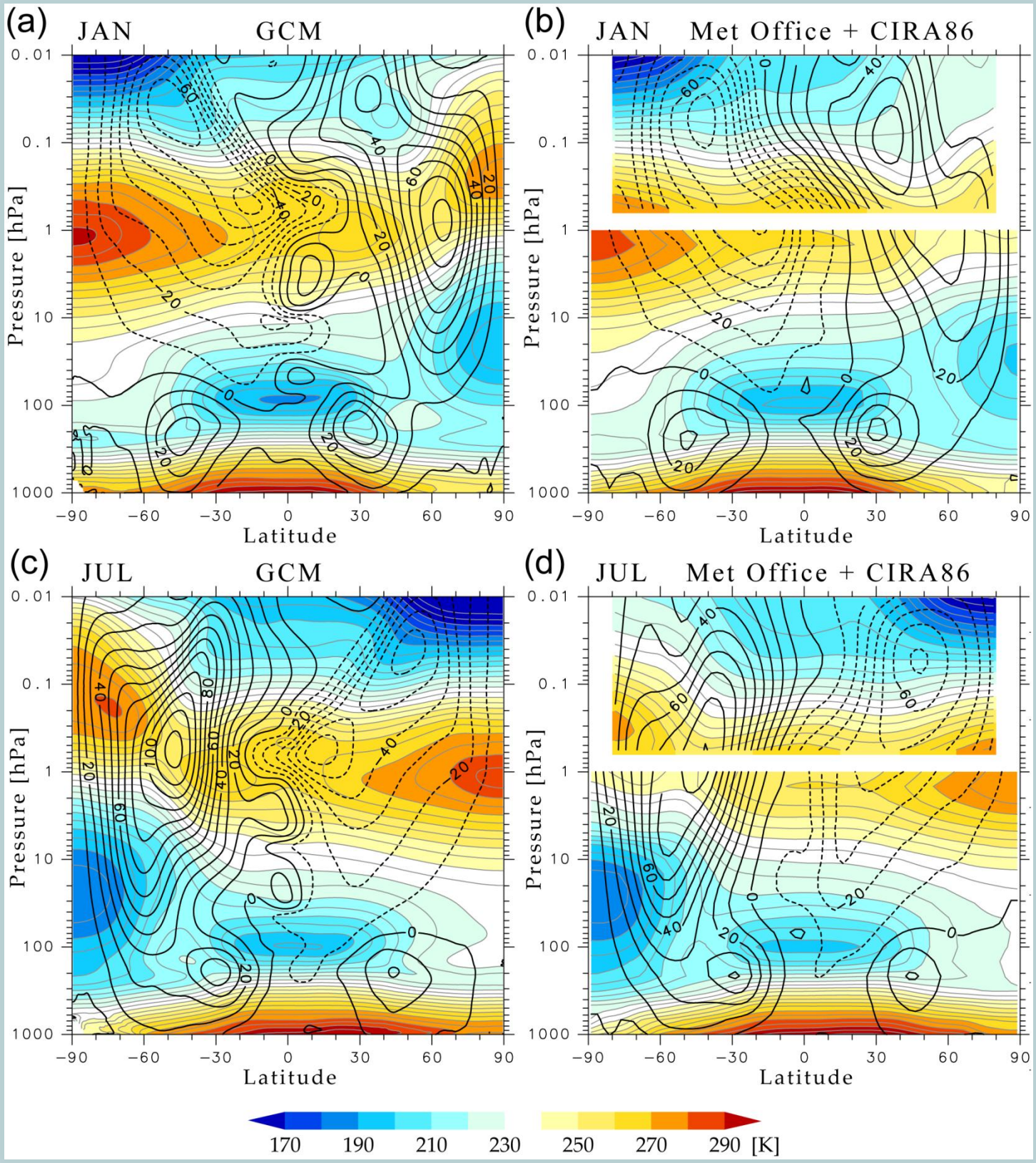

Fig. 1 Zonal mean zonal wind (contours) and temperature (color and thin contours) in (a,b) January and (c,d) July. (a,c) GCM, (b,d) Met Office+CIRA86. Contour intervals are 10 m s^{-1} and 5 K. Met Office data are averaged over 1994–2001 and displayed below 1 hPa.

Precipitation

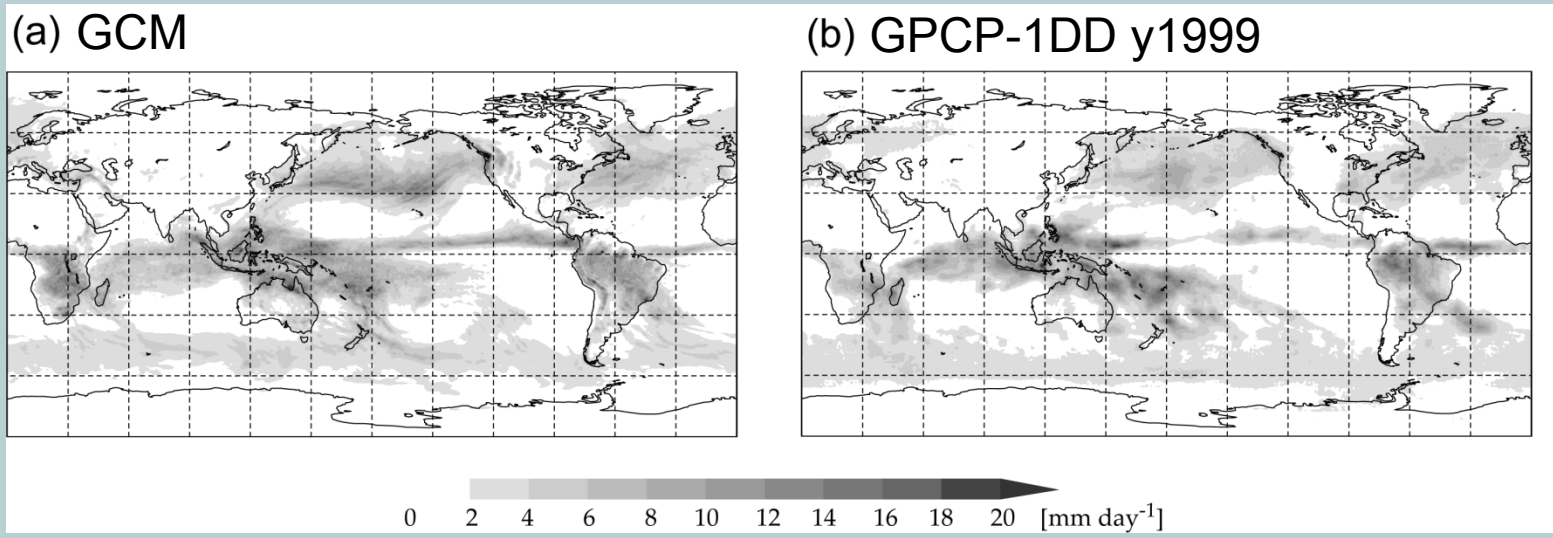

Fig. 2 January mean precipitation

GW spectra

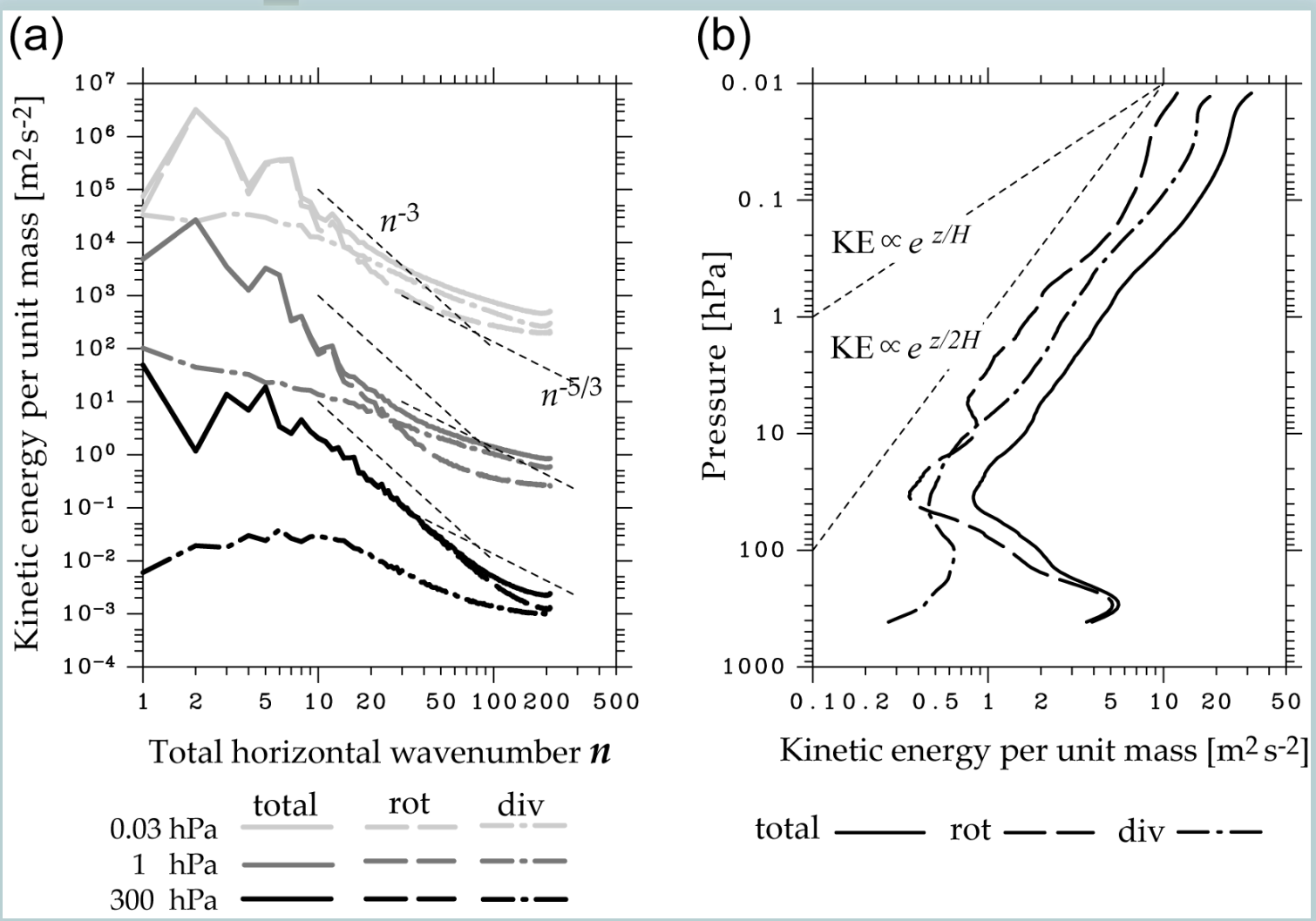

Fig. 3 (a) Total horizontal wavenumber spectra of horizontal kinetic energy. Results at 1 hPa and 0.03 hPa are multiplied by 100 and 10000, respectively.
(b) Vertical profile of horizontal kinetic energy integrated over n = 16–213 shown as an average over January 1–10.

E-P flux analysis January

DivF due to PW is dominant in the equator side of PNJ below about 60 km.

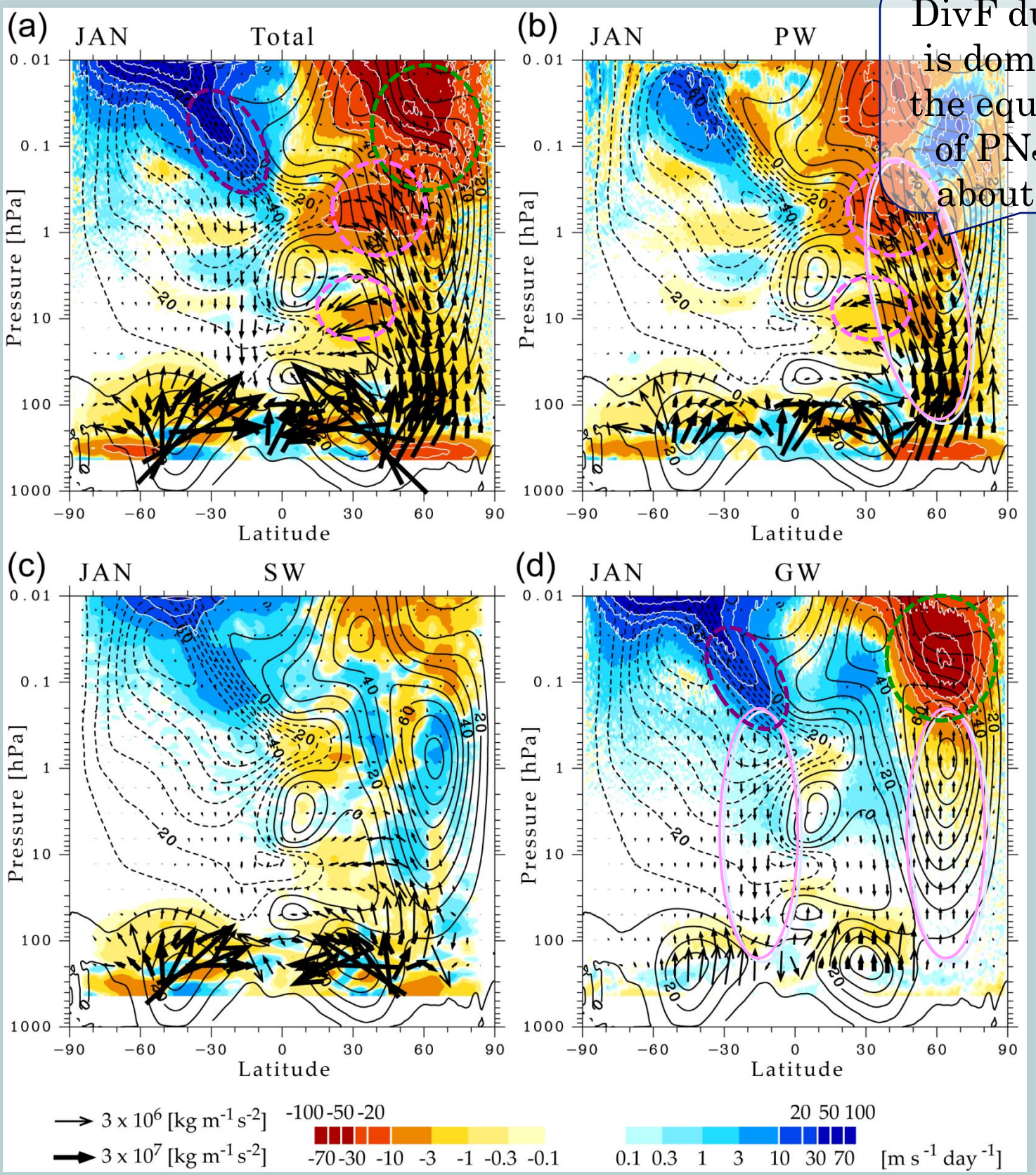

Fig. 4 E-P flux vectors (arrows) and eastward accelerations of zonal mean zonal wind due to divergence of E-P flux (colors) for January (average). (a) Total wave components, (b) PW group (s1-3), (c) SW group(n1-42), (d) GW group(n43-213). Scales of arrows are modified for clarity. Color scale is logarithmic. Contours denote zonal mean zonal wind in 10 m s^{-1} intervals.

E-P flux analysis July

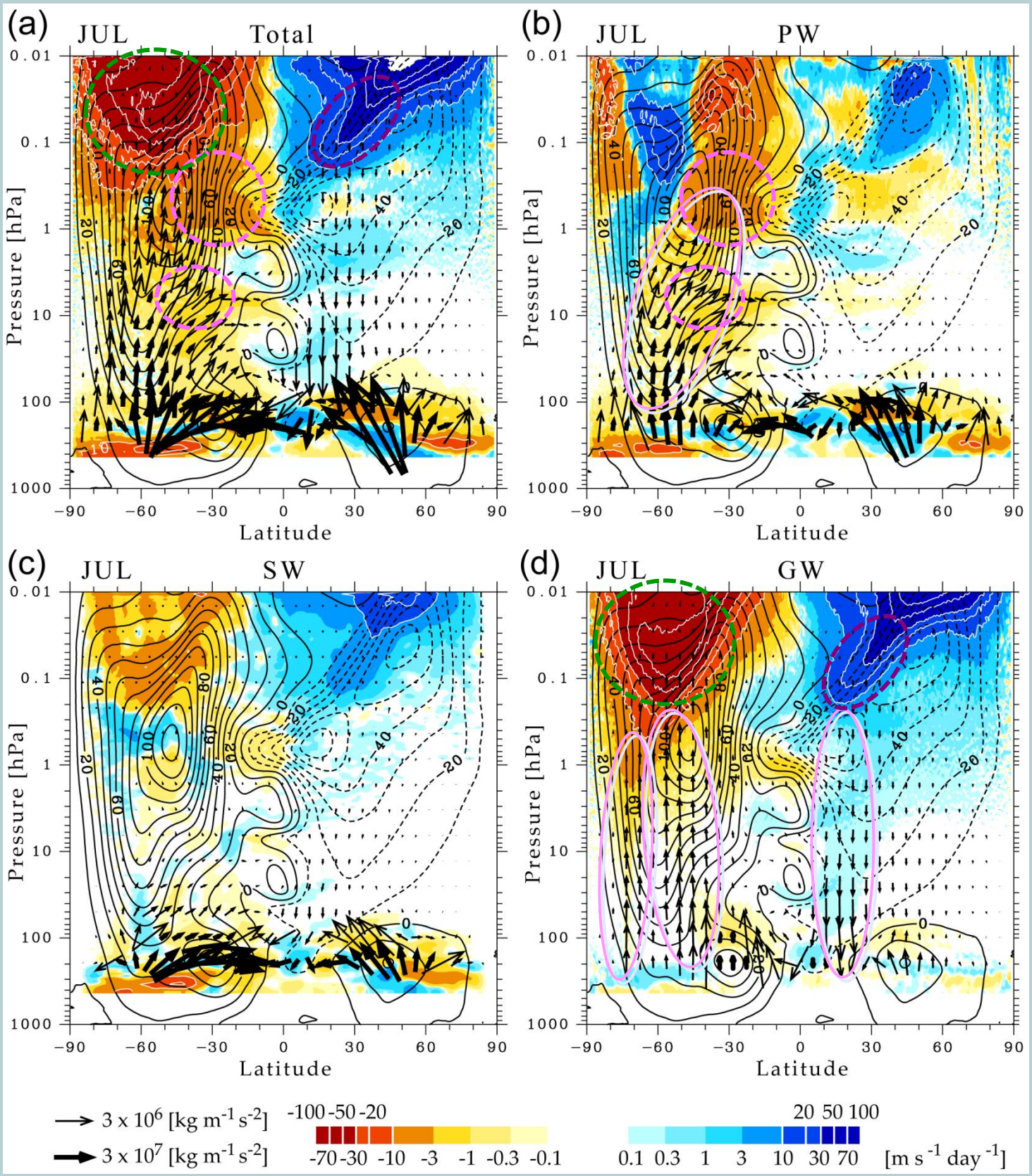

Fig. 5 E-P flux vectors (arrows) and eastward accelerations of zonal mean zonal wind due to divergence of E-P flux (colors) for July (average). (a) Total wave components, (b) PW group, (c) SW group, (d) GW group. Scales of arrows are modified for clarity. Color scale is logarithmic. Contours denote zonal mean zonal wind in 10 m s^{-1} intervals.

Meridional momentum flux

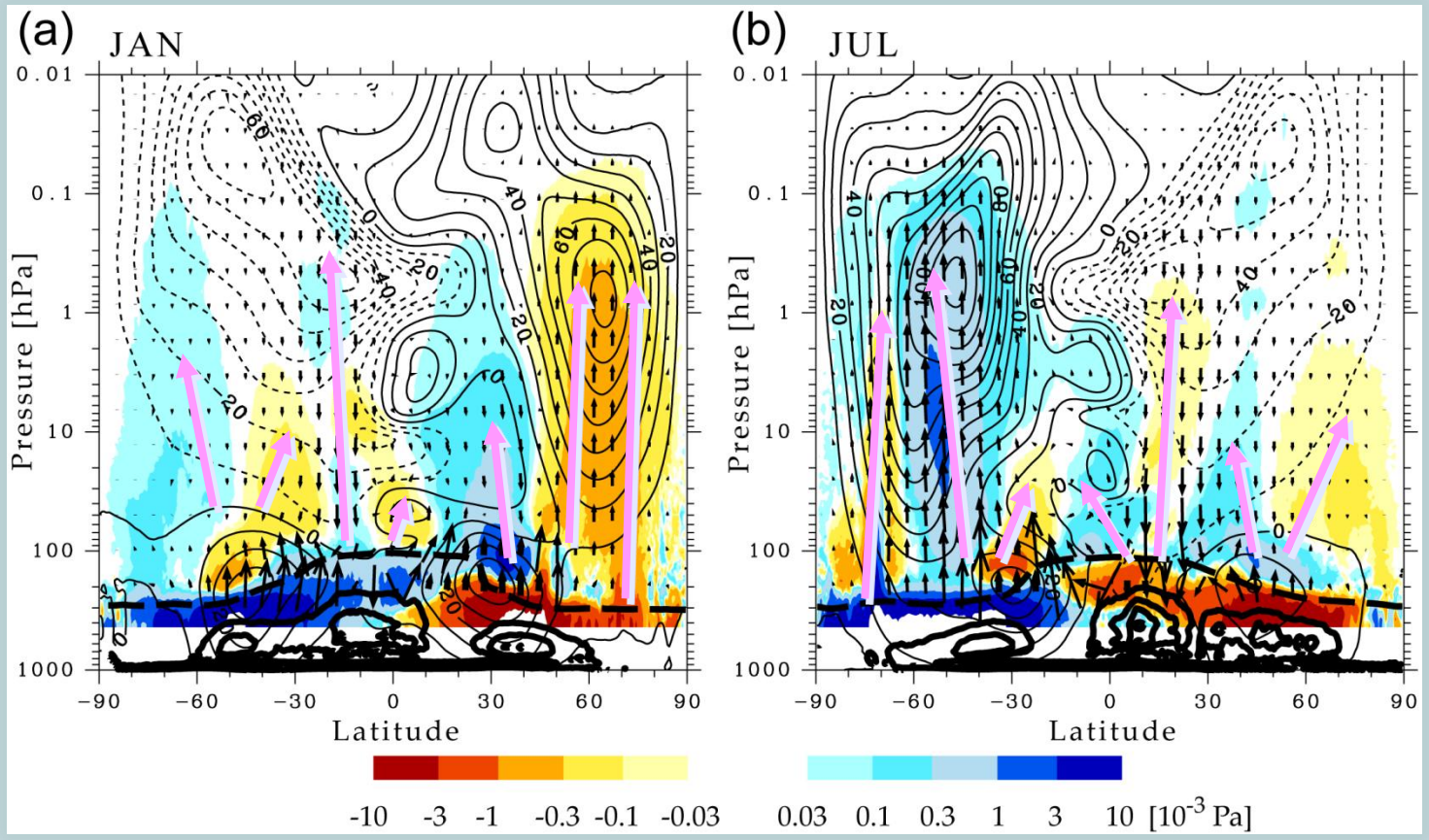

Fig. 6 Zonal mean vertical flux of meridional momentum ($r_0 v'w'$) associated with $n \geq 43$ waves and zonal mean zonal wind (contours) in (a) January and (b) July. Bold dashed line denotes the tropopause, and solid contour lines denote monthly average values of zonal mean condensational heating rate in the troposphere (cumulus + large-scale condensation, contour interval of 1 K day^{-1}).

Snapshot of GWs at 140E

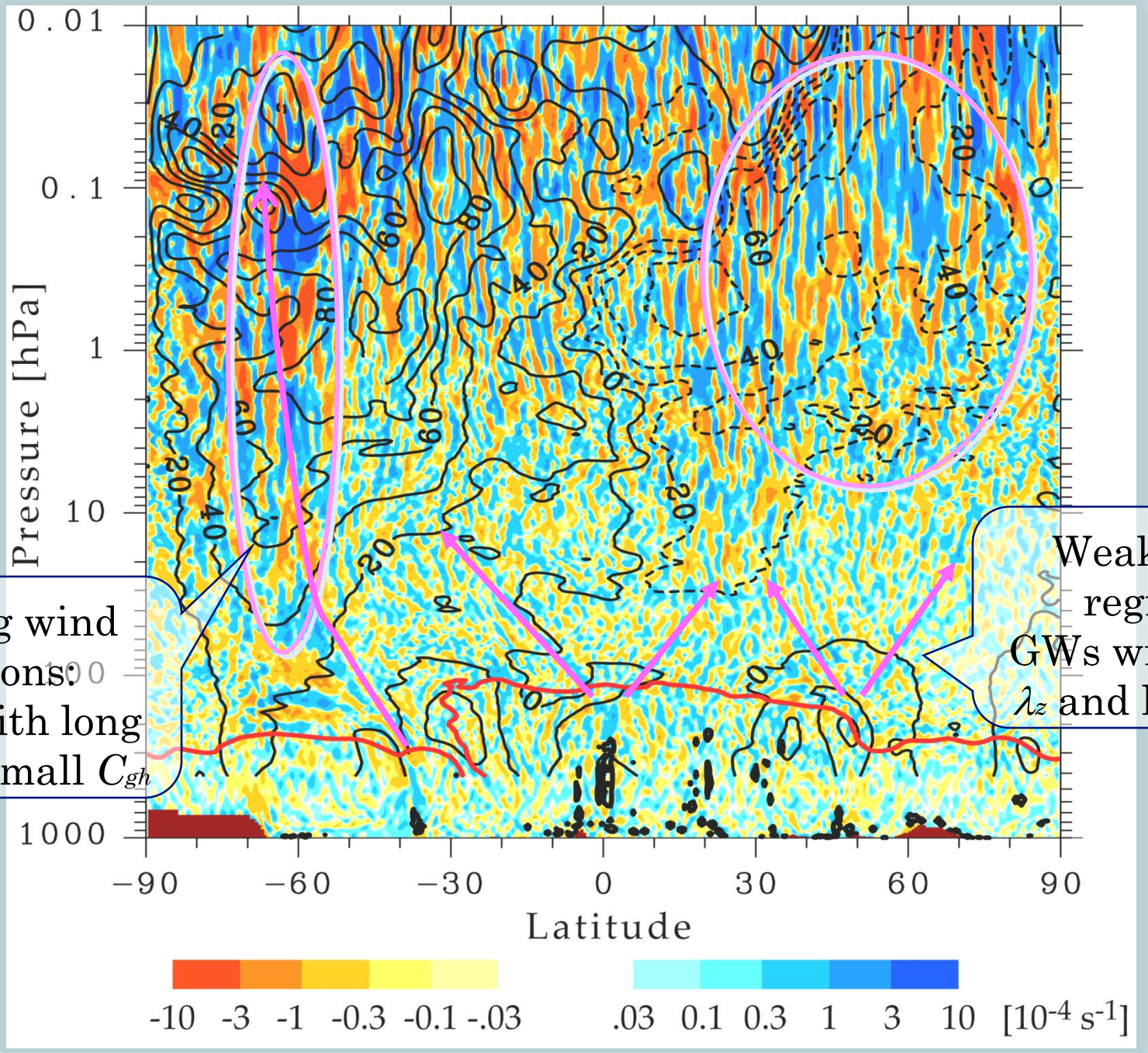

Fig. 7 Meridional cross-section of unfiltered instantaneous horizontal wind divergence (colors in logarithmic scale) and background zonal wind (contours) at 140°E on July 1 (0000 UTC). Bold red line denotes the tropopause. Solid contour lines denote condensational heating rate in the troposphere (cumulus + large-scale condensation, contour interval of 1 K day^{-1}). Contours of zonal wind and tropopause height are suppressed below 400 hPa because the horizontal spherical low-pass filter is unavailable due to topography. Surface topography is indicated in brown.

$\hat{\omega}$

GWs over South Andes

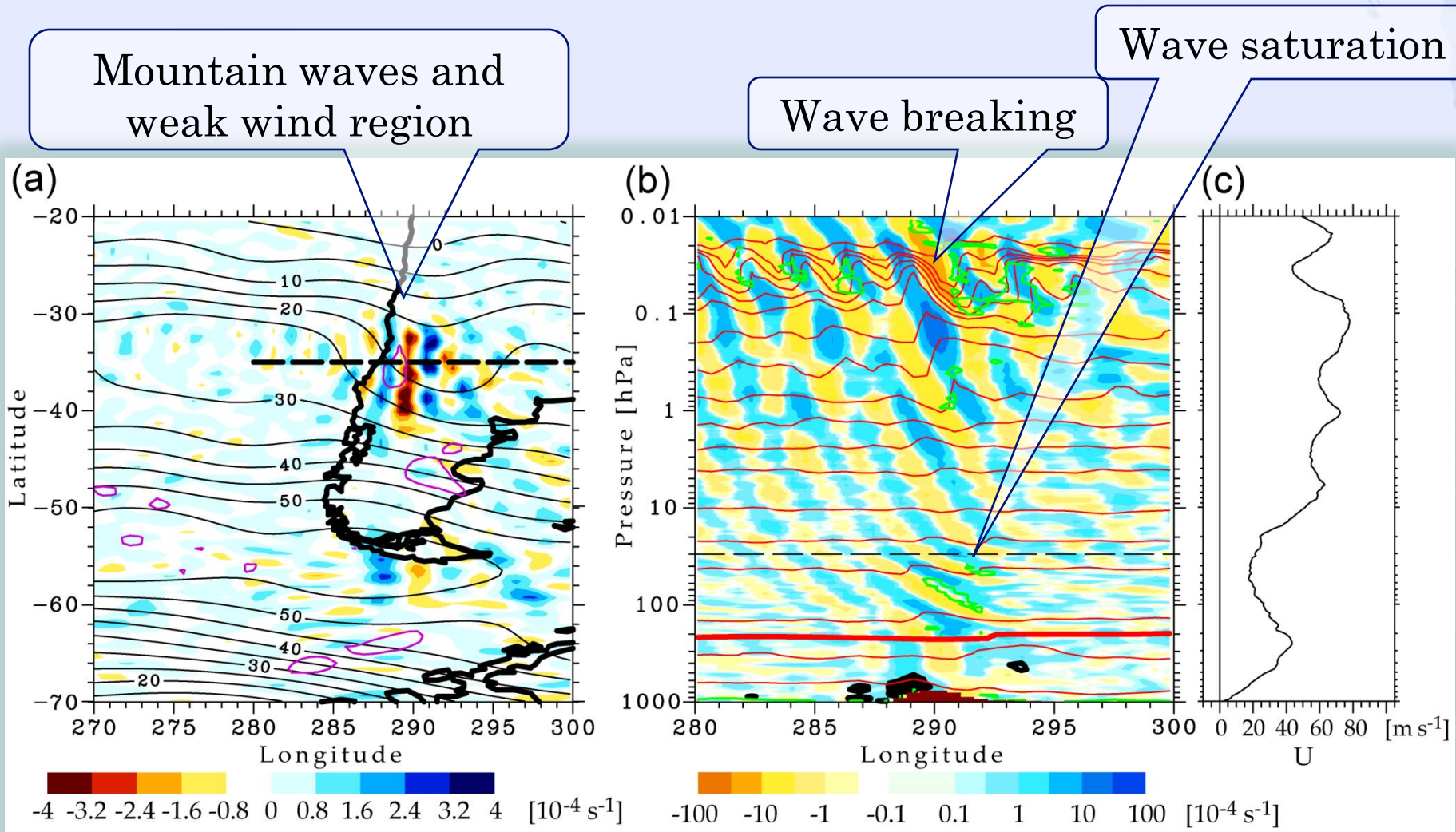

Fig. 8 (a) Divergence of unfiltered horizontal wind (color) and background zonal wind (black contour lines) at 30 hPa on July 5 (1000 UTC). Pink lines denote 1 mm h^{-1} contours of precipitation. (b) Divergence of unfiltered horizontal wind (color, logarithmic scale) and unfiltered potential temperature (red lines) at 35°S. Bold red line near 200 hPa denotes the tropopause. Regions enclosed by green lines have $Ri < 0.25$. Solid black contours denote condensational heating rate in the troposphere (cumulus + large-scale condensation, contour interval of 0.5 K h^{-1}). Brown denotes the surface topography at 290°E. (c) Background zonal wind at 35°S averaged over 280–300°E.

	λx [km]	λz [km]	$\lvert f/\hat{\omega}\rvert$	c_x [m s^{-1}]	c_{gz} [km h^{-1}]	U [m s^{-1}][a]	N [s^{-1}][b]
ORO	245	6.4	0.15	-1.6	2.0	20.0	0.0211

[a] Background zonal wind (average in vicinity of gravity waves)
[b] Brunt-Väisälä frequency (average in vicinity of gravity waves)

GWs from jet stream

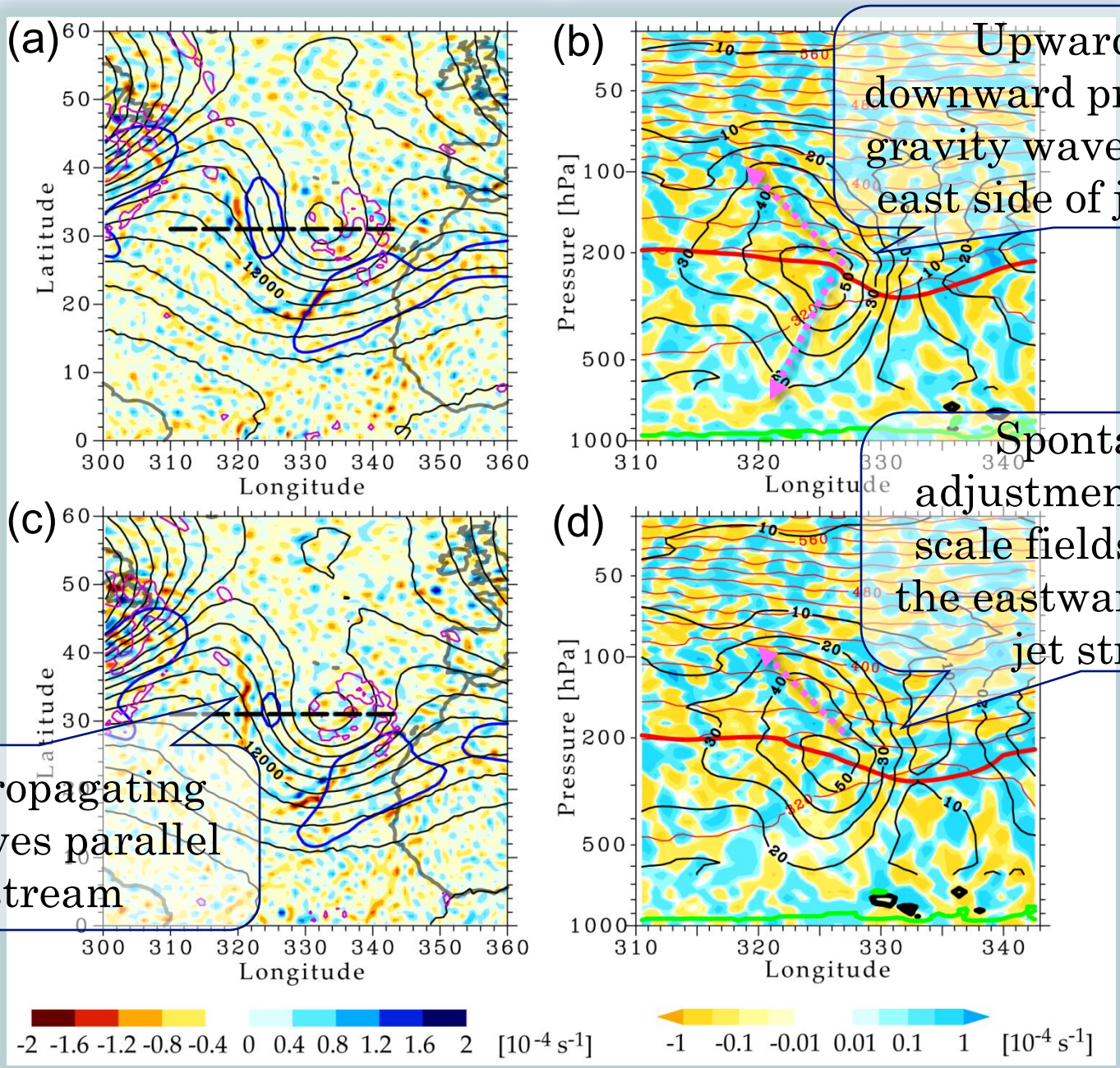

Upward and downward propagating gravity waves from the east side of jet stream

Spontaneous adjustment of large-scale fields including the eastward traveling jet stream?

Upward propagating gravity waves parallel to jet stream

Fig. 9 (a,c) Horizontal distribution of unfiltered horizontal wind divergence at 100 hPa (color), background geopotential height (black contour lines), 50 m s^{-1} isotach (blue contour lines) at 200 hPa, and precipitation (pink contour lines, interval of 1 mm h^{-1}). (b,d) Longitude–pressure cross-section at 31°N (bold dashed line in left panels) for unfiltered horizontal wind divergence (color, logarithmic scale), background absolute wind speed (black contour lines), unfiltered potential temperature (red contour lines), moist heating (bold black contour lines), Ri = 0.25 (green contour lines), tropopause (bold red lines). (a,b) Jan 4, 2200 UTC, (c,d) 2500 UTC.

	λx [km]	λz [km]	$\lvert f/\hat{\omega} \rvert$	c_x [m s^{-1}]	c_{gz} [km h^{-1}]	U [m s^{-1}]^a	N [s^{-1}]^b
JETup	262	2.2	0.42	+8.0	0.18	15.4	0.0196
JETdw	262	2.9	0.63	+4.7	-0.13	9.8	0.0087